ACS Sustainable Chemistry & Engineering

Research Article

Cite This: ACS Sustainable Chem. Eng. 2019, 7, 6802−6812

pubs.acs.org/journal/ascecg

Mechanochemical Synthesis of Ca- and Mg-Double Salt Crystalline Materials Using Insoluble Alkaline Earth Metal Bearing Minerals

Lohit Sharma, Daniyal Kiani, Kenneth Honer, and Jonas Baltrusaitis*

Department of Chemical and Biomolecular Engineering, Lehigh University, B336 Iacocca Hall, 111 Research Drive, Bethlehem, Pennsylvania 18015, United States

ABSTRACT: Sustainable, liquid-assisted grinding—mechanochemical synthesis—of crucial nutrient containing compounds, namely, Ca- and Mg-struvites ($CaNH_4PO_4{\cdot}H_2O$ and $MgNH_4PO_4{\cdot}6H_2O$) and complex double salts ($Ca(NH_4)_2(HPO_4)_2{\cdot}H_2O$ dimorph B, $Mg(NH_4)_2(HPO_4)_2{\cdot}4H_2O$ dimorph A), was performed. These compounds were synthesized using solid crystalline monoammonium phosphate ($NH_4H_2PO_4$, MAP) and low solubility common calcium and magnesium minerals, such as hydroxides, carbonates, and oxides. Powder X-ray diffraction showed single crystalline phase materials. Properties of the synthesized compounds were studied by thermogravimetric analysis/differential scanning calorimetry (TGA/DSC), Raman spectroscopy, and dynamic vapor sorption (DVS). TGA results showed that Ca-struvite was the most thermally robust, followed by Ca- and Mg-complex double salts and Mg-struvite. The decomposition of samples with release of NH_3 was marked by peaks in the DSC profiles at 190 °C for both complex double salts and a broad DSC shoulder at 186 °C was observed for struvites. Raman spectroscopy showed the presence of distorted PO_4^{3-} bands due to protonation of the phosphate species and multiple binding environments. DVS measurements showed that these compounds deliquesced at very high relative humidity conditions (~90%), which in some cases led to significant changes in the dominant crystalline phase.

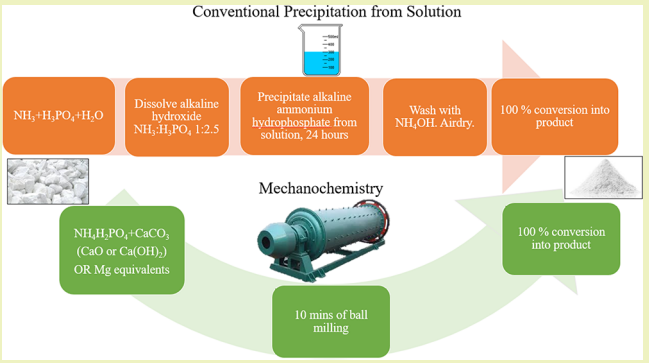

KEYWORDS: *Nutrients, Ammonium, Nitrogen fertilizers, Sustainable synthesis, Solubility, Mechanochemistry*

INTRODUCTION

As the agricultural community and fertilizer industry alike prepare for the challenges of soil nutrient depletion, rising food demand,[1−8] and adverse environmental impacts of over-fertilization,[8−14] the need for sustainable fertilizers, such as those partially or fully produced from inorganic rock, has come into focus in recent years.[3,15−17] One embodiment of the need for sustainable, economical fertilizers is the situation in Eastern Uganda, where it has been noted that urea in the region costs up to five times as much as in the United States.[18] Although, major plantations can afford these costs, small farms struggle to afford these expensive fertilizers. Another problem regarding the sustainability of widely used fertilizers lies within the fact that a majority of fertilizers only supply primary macronutrients (N, P, K) while leaving out other important secondary macronutrients (Ca, Mg, S).[19,20] Some of these secondary macronutrients, such as the divalent cations of calcium and magnesium, have been regarded as a critical secondary nutrients for over a hundred years.[21,22] Calcium, while sometimes overlooked and left out of commercial NPK fertilizers, is known to assist many plant biological processes within cytoplasm and the cell wall.[23] Magnesium is the most prevalent divalent cation in cytosol and is critical in the formation of many plant enzymes.[24] An immediate challenge arises since both calcium and magnesium are immobilized in insoluble minerals. Although magnesium is a common constituent of many minerals, comprising 2% of the earth's crust, most soil magnesium (~98%) is incorporated in the crystal lattice structure of low solubility minerals and thus is not directly available for plant uptake.[25]

To keep up with modern agriculture and sustainable nutrient management,[8,26,27] developments in both slow release and enhanced efficiency fertilizer design and synthesis have recently experienced a strong rejuvenation. In particular, solvent-free mechanochemical methods have been utilized to prepare fertilizers containing major nutrients. Mechanochemistry has been recognized as an emerging green method of solid state material transformations, especially as it allows solvent-free modes of synthesis and is less energy intensive than other major industrial processes.[28−31] Traditional methods of producing N−P−K fertilizers that use NH_3 as a reactant typically produce 1400−2600 kg of CO_2 equivalent per kilogram of N fixed.[32,33] On the other hand, a typical industrial ball-mill requires 0.01−0.10 kWh/kg of solid (MAP, Mg-, Ca-precursors in this case) milled,[34,35] which translates to 0.005−0.05 kg of CO_2 equivalent per kilogram of solid milled. Soluble

Received: November 23, 2018
Revised: February 25, 2019
Published: March 5, 2019

DOI: 10.1021/acssuschemeng.8b06129
ACS Sustainable Chem. Eng. 2019, 7, 6802−6812

nutrient salts, such as $KH_2PO_4/NH_4H_2PO_4$ have mechanochemically been incorporated into insoluble matrixes of Al_2O_3[36] or clay minerals.[37,38] Potassium and magnesium from the corresponding hydroxides and nitrates have also been incorporated in slow release matrixes with SiO_2 or layered double hydroxides.[39−41] Other attempts utilized mechanochemistry to enhance nutrient release from otherwise insoluble minerals such as phlogopite[42] and chrysotile[43] with or without the corresponding coreactants to perform a double substitution reaction. Reactive mechanochemistry to make complex fertilizer materials using abundant magnesium or calcium minerals (oxides, hydroxides, and carbonates) has seldom been utilized. Nutrient containing waste, such as $FeSO_4$ and $ZnSO_4$, has mechanochemically been transformed by milling with $CaCO_3$ into the corresponding metal carbonates with a resulting ∼100% release rate in 2% citric acid solution.[44] $KMgPO_4$ was prepared by milling KH_2PO_4 and $Mg(OH)_2$ at a molar ratio of 1:1 for 120 min at mill rotational speeds of 500−600 rpm.[45] The same authors also synthesized $MgNH_4PO_4$ by milling $NH_4H_2PO_4$ and $Mg(OH)_2$ at a molar ratio of 1:1 for 120 min at mill rotational speeds of 300−700 rpm. Recent work utilized either magnesoum or calcium salts[46] or the corresponding oxide, hydroxide, and carbonate compounds[17] to mechanochemically obtain their corresponding urea adducts with improved nitrogen management.

The emphasis of this work is on creating complex fertilizer materials that incorporate both primary (N and P) and secondary (Mg, Ca) macronutrients in one crystalline unit using mechanochemistry. In particular, two complex fertilizer materials of interest are dimorph B of $Ca(NH_4)_2(HPO_4)_2{\cdot}H_2O$ and dimorph A of $Mg(NH_4)_2(HPO_4)_2{\cdot}4H_2O$, two highly soluble compounds combining three nutrients, such as Ca or Mg with N and P; however, challenges that faced their conventional synthesis are evident in Figure 1. The compounds

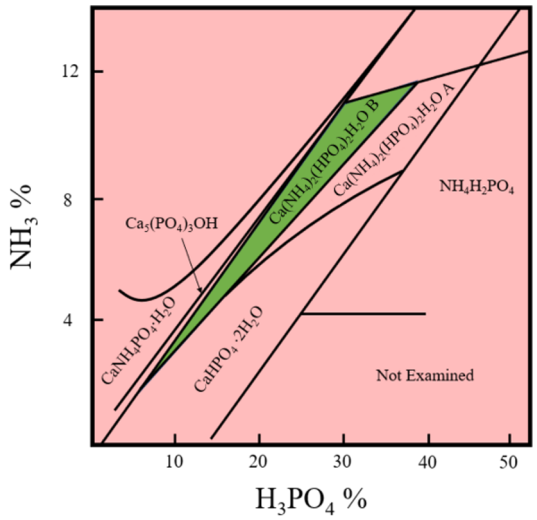

Figure 1. Adapted from ref 47. Copyright 1964 American Chemical Society.

were slowly precipitated out of aqueous solutions of NH_3, H_3PO_4, and alkaline salts of either magnesium or calcium. The process to precipitate dimorph B of $Ca(NH_4)_2(HPO_4)_2{\cdot}H_2O$ from solution took around a day, and a highly specific NH_3 to H_3PO_4 ratio of about 1 to 2.5 was needed to achieve the crystallization of the specific dimorph of the salt.[48] It was also later noted that a specific pH range between 5.3 and 8.0 was needed to produce the salt from solution.[49] Similar characteristics of precipitation were observed for dimorph A of $Mg(NH_4)_2(HPO_4)_2{\cdot}4H_2O$ in regards to duration of precipitation, pH requirements and NH_3: H_3PO_4 ratio.[50] When prepared using a conventional precipitation from solutions, both compounds had an impurity of monoammonium phosphate (MAP).[51] Interestingly, $Ca(NH_4)_2(HPO_4)_2{\cdot}H_2O$ was previously determined as a product from the reaction of diammonium phosphate (DAP) and alkaline soils.[52] $Ca(NH_4)_2(HPO_4)_2{\cdot}H_2O$ was found naturally in a Namibian cave where it is believed that bat excreta reacted with the phosphate compounds in the walls of the cave to produce the specific dimorph.[53] This suggests that double salt synthesis using natural magnesium and calcium bearing minerals should be feasible.

We utilized solid crystalline MAP—a very large volume solid fertilizer and chemical intermediate—as both nitrogen and phosphorus precursor, while using magnesium and calcium oxides, hydroxides, and carbonates as alkaline metal precursors via reactive milling. By adjusting precursor ratios, we were able to selectively obtain either Ca- or Mg-struvites ($CaNH_4PO_4{\cdot}H_2O$ or $MgNH_4PO_4{\cdot}6H_2O$) or the corresponding higher nitrogen and phosphorus content complex salts ($Ca(NH_4)_2(HPO_4)_2{\cdot}H_2O$ or $Mg(NH_4)_2(HPO_4)_2{\cdot}4H_2O$). Theoretical yields and product determination were determined from powder X-ray diffraction (pXRD) and further analysis of the synthesized compounds was conducted using thermogravimetric analysis (TGA)/differential scanning calorimetry (TGA/DSC) and Raman spectroscopy. Finally, environmental reactivity properties toward water vapor have been assessed using the dynamic vapor sorption (DVS) technique.

EXPERIMENTAL SECTION

Reagents and Solutions. Monoammonium phosphate, $NH_4H_2PO_4$ (MAP, 99.9%+, Fisher Scientific), MgO (99%+, Sigma-Aldrich), $Mg(OH)_2$ (95%, Acros Organics), $MgCO_3$ (500 grade, Acros Organics), $Ca(OH)_2$ (96%+, Sigma-Aldrich), CaO (reagent grade, Sigma-Aldrich) and $CaCO_3$(99%+, Acros Organics) powders were used as received.

Mechanochemistry and Crystal Structure Testing. In a typical procedure, a total of 200 mg to 400 mg sample of Ca or Mg precursor (oxide, hydroxide, or carbonate) and monoammonium phosphate (MAP, $NH_4H_2PO_4$) with the corresponding molar ratios were loaded into a 15 mL stainless steel jar together with three individual 8 mm stainless steel balls and grounded for up to 10 min at 26 Hz in a Retsch MM300 mixer mill. Liquid assisted grinding (LAG) was utilized due to the high crystalline water content in the products. All samples were air-dried before pXRD analysis.

Powder X-ray Diffraction (pXRD) Analysis. To determine the crystalline identity of the mechanochemical product and the overall conversion of the reactants (MAP, Ca- and Mg-hydroxides, oxides, carbonates, and water), pXRD analysis (Empyrean, PANalytical B.V.) was performed. The applied current was 40 mA and the applied voltage was 45 kV. The X-ray mirror that was used was a graded, flat Bragg−Brentano HD mirror, and the step size that was used for the measurements was 0.0131 degrees.

The three pXRD patterns that were obtained using the different calcium sources of $Ca(OH)_2$, $CaCO_3$, and CaO were matched against the theoretical line graph of dimorphs A and B of $Ca(NH_4)_2(HPO_4)_2{\cdot}H_2O$ (PDF 20−204). Likewise, the patterns that were obtained from $Mg(OH)_2$, $MgCO_3$, and MgO were also compared to the theoretical line graphs of dimorphs A and B of $Mg(NH_4)_2(HPO_4)_2{\cdot}4H_2O$.[54−57] While the crystal structure of neither compound is fully known, experimental pXRD patterns have been reported and shown in Figure 2.[47,58,59] Ca- or Mg-struvites ($CaNH_4PO_4{\cdot}H_2O$[47] or $MgNH_4PO_4{\cdot}6H_2O$[60]) were indexed according to their simulated pXRD patterns

DOI: 10.1021/acssuschemeng.8b06129
ACS Sustainable Chem. Eng. 2019, 7, 6802−6812

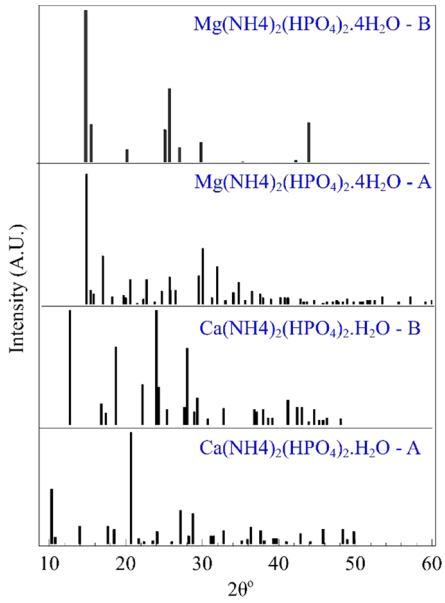

Figure 2. Theoretical XRD peak positions of $Ca(NH_4)_2(HPO_4)_2 \cdot H_2O$ and $Mg(NH_4)_2(HPO_4)_2 \cdot 4H_2O$ dimorphs.

obtained from the reported crystal structures. In the case of Mg–complex salt, (indicated in the text) reactant peaks from unreacted monoammonium phosphate were also observed. On the basis ofthis observation, it can be determined that very high conversion rates occurred during milling slightly lower conversion took place for Mg–complex salts, most likely due to its more soluble nature of the Mg precursors.[17]

Thermal Analysis. Simultaneous measurement of weight change (TGA) and differential heat flow (DSC) was assessed using SDT-Q600, TA Instruments. During TG/DSC measurements, a heating rate of 10 °C/min was used under N_2 flow of 100 mL/min.

Raman Spectroscopy. Raman spectra and spectral maps were acquired using WITec alpha300R confocal Raman microscope using a 532 nm laser and ×100 objective. Laser intensity at the sample was ~54 mW.

Dynamic Vapor Sorption Analysis. The DVS Intrinsic (Surface Measurement Systems Ltd., USA) equipped with SMS Ultrabalance with a mass resolution of ±0.1 μg was used to obtain ramping and equilibrium water vapor sorption isotherms. Approximately 5 mg of powder was placed in an aluminum pan in the apparatus and initially dried over 600 min with a stream of dry nitrogen to establish a dry mass at 25 °C. The dry mass was calculated after the end of first drying stage (~0% RH). The sorption cycle experiments were performed from 0% relative humidity (RH) to 90% RH in a step of 10% in a preprogrammed sequence, before decreasing to 0% RH in a reverse order. The instrument maintained a constant target RH until the moisture content change per minute (dm/dt) was less than 0.002% per minute over a 10 min period. All samples for DVS analysis were synthesized mechanochemically from the corresponding hydroxides and MAP except Ca-struvite, $CaNH_4PO_4 \cdot H_2O$, which was synthesized using CaO. MAP was milled for the same period of time before analysis for comparison. DVS curves were obtained in at least triplicate from three independent samples.

RESULTS AND DISCUSSION

Mechanochemical Synthesis and pXRD of $Ca(NH_4)_2(HPO_4)_2 \cdot H_2O$ and $Mg(NH_4)_2(HPO_4)_2 \cdot 4H_2O$. A 2-fold excess of both Ca- or Mg-bearing minerals was necessary to achieve the complex magnesium double salt, $Mg(NH_4)_2(HPO_4)_2 \cdot 4H_2O$ and $Ca(NH_4)_2(HPO_4)_2 \cdot H_2O$, formation according to eqs 1 through 6

$$Mg(OH)_2 + 2NH_4H_2PO_4 + 2H_2O \rightarrow Mg(NH_4)_2(HPO_4)_2 \cdot 4H_2O \quad (1)$$

$$MgO + 2NH_4H_2PO_4 + 3H_2O \rightarrow Mg(NH_4)_2(HPO_4)_2 \cdot 4H_2O \quad (2)$$

$$MgCO_3 + 2NH_4H_2PO_4 + 3H_2O \rightarrow Mg(NH_4)_2(HPO_4)_2 \cdot 4H_2O + CO_2 \quad (3)$$

$$Ca(OH)_2 + 2NH_4H_2PO_4 \rightarrow Ca(NH_4)_2(HPO_4)_2 \cdot H_2O + H_2O \quad (4)$$

$$CaO + 2NH_4H_2PO_4 \rightarrow Ca(NH_4)_2(HPO_4)_2 \cdot H_2O \quad (5)$$

$$CaCO_3 + 2NH_4H_2PO_4 \rightarrow Ca(NH_4)_2(HPO_4)_2 \cdot H_2O + CO_2 \quad (6)$$

Stoichiometrically, magnesium complex salt requires the addition of water molecules to yield four crystalline water molecules. This was done by adding a few droplets of liquid water into the reaction mixture to perform liquid assisted grinding. As shown in Figure 3, solid products resulting from

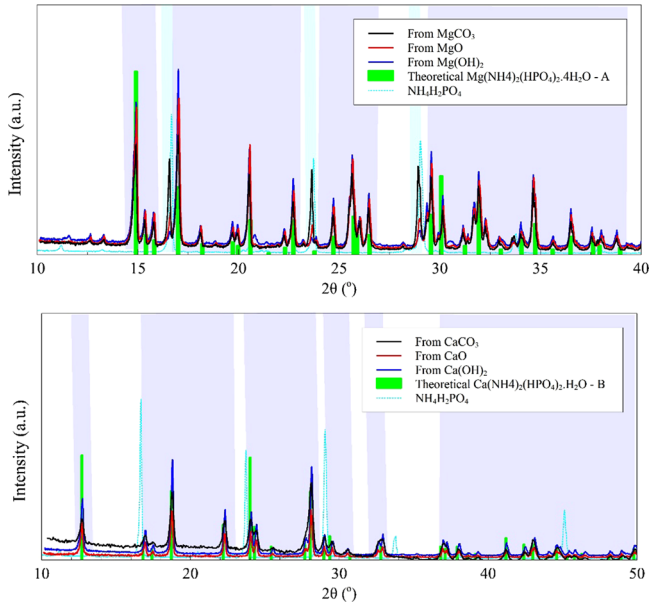

Figure 3. Comparison of pXRD patterns of $Mg(NH_4)_2(HPO_4)_2 \cdot 4H_2O$ (top) and $Ca(NH_4)_2(HPO_4)_2 \cdot H_2O$ (bottom) resulting after mechanochemical treatment of (top) $Mg(OH)_2$, MgO, and $MgCO_3$ and (bottom) $Ca(OH)_2$, CaO, and $CaCO_3$ with $NH_4H_2PO_4$ using 1:2 molar ratio. The product XRDs have been slightly offset vertically for clarity. Peaks corresponding to $Mg(NH_4)_2(HPO_4)_2 \cdot 4H_2O$ dimorph A and $Ca(NH_4)_2(HPO_4)_2 \cdot H_2O$- dimorph B are highlighted in royal blue, and unreacted MAP($NH_4H_2PO_4$) is highlighted in cyan.

LAG of $Mg(OH)_2$, MgO, and $MgCO_3$ with MAP indeed yielded mostly complex double salt $Mg(NH_4)_2(HPO_4)_2 \cdot 4H_2O$. Interestingly, a complete conversion of reactants at 2:1 mineral/MAP reactant ratio was only achieved to yield $Ca(NH_4)_2(HPO_4)_2 \cdot H_2O$, as shown in Figure 3, using LAG during CaO and $CaCO_3$ milling with MAP, as summarized in Table 1. While the stoichiometry of reactions 5 and 6 does not

DOI: 10.1021/acssuschemeng.8b06129
ACS Sustainable Chem. Eng. 2019, 7, 6802–6812

Table 1. LAG Synthesis of Ca- and Mg-Containing Double Salts ($Ca(NH_4)_2(HPO_4)_2{\cdot}H_2O$ or $Mg(NH_4)_2(HPO_4)_2{\cdot}4H_2O$) from the Corresponding Ca- and Mg-Hydroxides, Oxides, and Carbonates

mineral	molar ratio (mineral/MAP)	LAG	major product from pXRD analysis
$Mg(OH)_2$	1:2	yes	$Mg(NH_4)_2(HPO_4)_2{\cdot}4H_2O$
$Mg(OH)_2$	1:2	no	no reaction
MgO	1:2	yes	$Mg(NH_4)_2(HPO_4)_2{\cdot}4H_2O$
MgO	1:2	no	no reaction
$MgCO_3$	1:2	yes	$Mg(NH_4)_2(HPO_4)_2{\cdot}4H_2O$
$MgCO_3$	1:2	no	no reaction
$Ca(OH)_2$	1:2	yes	$Ca(NH_4)_2(HPO_4)_2{\cdot}H_2O$
$Ca(OH)_2$	1:2	no	$Ca(NH_4)_2(HPO_4)_2{\cdot}H_2O$
CaO	1:2	yes	$Ca(NH_4)_2(HPO_4)_2{\cdot}H_2O$
CaO	1:2	no	no reaction
$CaCO_3$	1:2	yes	$Ca(NH_4)_2(HPO_4)_2{\cdot}H_2O$
$CaCO_3$	1:2	no	no reaction

require water to make $Ca(NH_4)_2(HPO_4)_2{\cdot}H_2O$, an intermediate hydroxylated compound, such as $Ca(OH)_2$ can likely be forming to then be converted into the final product. This is confirmed when $Ca(OH)_2$ is converted with or without LAG into $Ca(NH_4)_2(HPO_4)_2{\cdot}H_2O$, as shown in Table 1. This also implies that CaO and $CaCO_3$ are less reactive and LAG induces reactivity by mobilizing boundaries of the crystals, consistent with recent experiments.[61−64]

Varying amounts of unreacted MAP were observed in pXRD analysis Figure 3 in all cases of the Mg−complex salt. Having said that, the case of the most soluble Mg precursor used in this study, for example, $MgCO_3$, had the highest quantity of unreacted MAP, regardless of varying ratios, the reactant milling time, and the added water amount. On the other hand, in the case of Ca-containing product, all precursors resulted in extremely high conversion, and exclusively produced $Ca(NH_4)_2(HPO_4)_2{\cdot}H_2O$, dimorph B, as the product. A comparison of the product in the case of all Ca precursors vs the product from the Mg precursors shows that the Ca-containing product had higher purity and matched the theoretical XRD very closely. The Mg−complex salt showed some peaks that did not match the theoretical XRD of dimorph A and upon further analysis were attributed to unreacted MAP, while the three peaks below 15° were unresolved and most likely occurred from an impurity or were from the desired product. Interesting to note here is that all Ca precursors were less soluble compared to the their corresponding Mg counterparts, which is most likely the reason for the higher conversion in the Ca case. The strongly solubility-dependent phase production can also be seen within the Mg-containing complex salts, as the most soluble $MgCO_3$ (vs MgO, $Mg(OH)_2$) produced the lowest yield of the product.

Mechanochemical Synthesis and pXRD of $CaNH_4PO_4{\cdot}H_2O$ and $MgNH_4PO_4{\cdot}6H_2O$. Stoichiometric amounts of both Ca- or Mg-bearing minerals were necessary to achieve the complex magnesium double (struvite) salt, $MgNH_4PO_4{\cdot}6H_2O$ and $CaNH_4PO_4{\cdot}H_2O$, formation according to eqs 7 through 12.

$$Mg(OH)_2 + NH_4H_2PO_4 + 4H_2O \rightarrow MgNH_4PO_4{\cdot}6H_2O \quad (7)$$

$$MgO + NH_4H_2PO_4 + 5H_2O \rightarrow MgNH_4PO_4{\cdot}6H_2O \quad (8)$$

$$MgCO_3 + NH_4H_2PO_4 + 5H_2O \rightarrow MgNH_4PO_4{\cdot}6H_2O + CO_2 \quad (9)$$

$$Ca(OH)_2 + NH_4H_2PO_4 \rightarrow CaNH_4PO_4{\cdot}H_2O + H_2O \quad (10)$$

$$CaO + NH_4H_2PO_4 \rightarrow CaNH_4PO_4{\cdot}H_2O \quad (11)$$

$$CaCO_3 + NH_4H_2PO_4 \rightarrow CaNH_4PO_4{\cdot}H_2O + CO_2 \quad (12)$$

Stoichiometrically, magnesium double salt requires the addition of even water molecules to obtain $Mg(NH_4)_2(HPO_4)_2{\cdot}4H_2O$ to yield the six-crystalline water molecules form $MgNH_4PO_4{\cdot}6H_2O$. This was also done by adding a few droplets of liquid water into the reaction mixture to perform liquid assisted grinding. As shown in Figure 3 left, solid products resulting from the LAG of $Mg(OH)_2$, MgO, and $MgCO_3$ with MAP indeed yielded a complex double struvite salt $MgNH_4PO_4{\cdot}6H_2O$. No unreacted MAP was observed in pXRD in either case, but reactions always took place only with water added as shown in Table 2.

A complete conversion of reactants at 1:1 mineral/MAP reactant ratio was only achieved to yield $CaNH_4PO_4{\cdot}H_2O$, as shown in Figure 4 right, using LAG during $Ca(OH)_2$ and CaO

Table 2. LAG Synthesis of Ca- and Mg-Containing Double Salts ($CaNH_4PO_4{\cdot}H_2O$ or $MgNH_4PO_4{\cdot}6H_2O$) from the Corresponding Ca- and Mg-Hydroxides, Oxides, and Carbonates

mineral	molar ratio (mineral/MAP)	LAG	product from pXRD analysis	remarks
$Mg(OH)_2$	1:1	yes	$MgNH_4PO_4{\cdot}6H_2O$	
$Mg(OH)_2$	1:1	no	no reaction	
MgO	1:1	yes	$MgNH_4PO_4{\cdot}6H_2O$	
MgO	1:1	no	no reaction	
$MgCO_3$	1:1	yes	$MgNH_4PO_4{\cdot}6H_2O$	
$MgCO_3$	1:1	no	no reaction	
$Ca(OH)_2$	1:1	yes	$CaNH_4PO_4{\cdot}H_2O$	
$Ca(OH)_2$	1:1	no	$Ca(NH_4)_2(HPO_4)_2{\cdot}H_2O$	complex double salt formed
CaO	1:1	yes	$CaNH_4PO_4{\cdot}H_2O$	
CaO	1:1	no	no reaction	
$CaCO_3$	1:1	yes	unknown product	product does not match the pXRD of $Ca(NH_4)_2(HPO_4)_2{\cdot}H_2O$, $CaNH_4PO_4{\cdot}H_2O$ or $CaNH_4PO_4{\cdot}7H_2O$
$CaCO_3$	1:1	no	no reaction	

DOI: 10.1021/acssuschemeng.8b06129
ACS Sustainable Chem. Eng. 2019, 7, 6802−6812

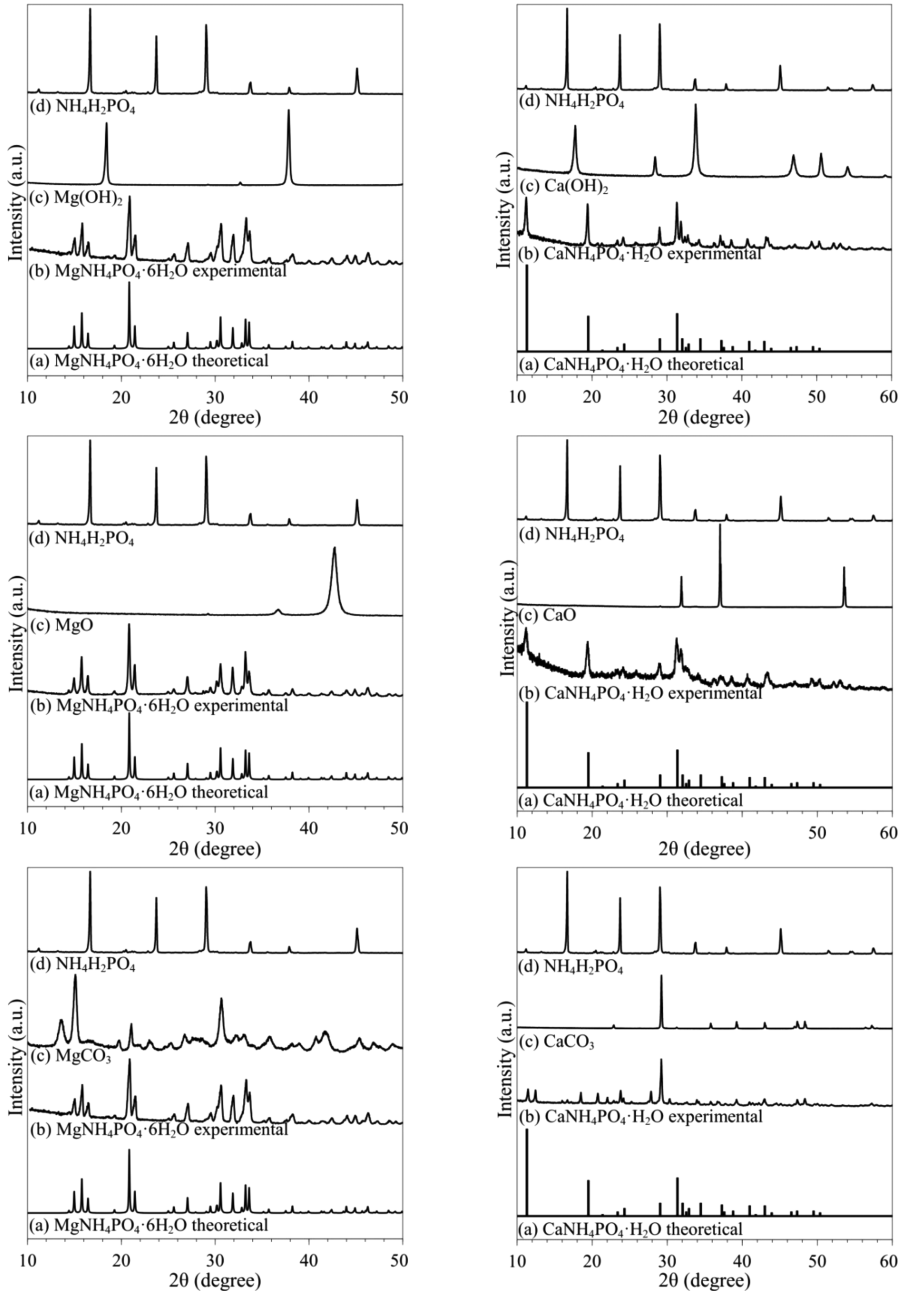

Figure 4. pXRD patterns of $CaNH_4PO_4·H_2O$ or $MgNH_4PO_4·6H_2O$ resulting after mechanochemical treatment of (right) $Ca(OH)_2$, CaO, $CaCO_3$ and (left) $Mg(OH)_2$, MgO, and $MgCO_3$ with $NH_4H_2PO_4$ using 1:1 molar ratio.

milling with MAP, as summarized in Table 2. While the stoichiometry of reaction 11 does not require water to make $CaNH_4PO_4·H_2O$, similarly to more complex double salts, an intermediate hydroxylated compound, such as $Ca(OH)_2$ can likely be forming to be converted into the final product in the case of CaO conversion. This is confirmed when $Ca(OH)_2$ is converted with LAG into $CaNH_4PO_4·H_2O$, as shown in Table 2. Interestingly, however, is that $Ca(OH)_2$ without LAG and 1:1 mineral/MAP reactant ratio was converted to $Ca(NH_4)_2(HPO_4)_2·H_2O$ with traces of $Ca(OH)_2$ as shown in the pXRD (not shown here). We suggest that $Ca(NH_4)_2(HPO_4)_2·H_2O$ is thermodynamically more favorable when abundant moisture is available during the milling of $Ca(OH)_2$. CaO and $CaCO_3$ with no LAG yielded no product, while $CaCO_3$ with LAG yielded a pXRD pattern that did not match any of the potential products, such as $Ca(NH_4)_2(HPO_4)_2·H_2O$, $CaNH_4PO_4·H_2O$, or $CaNH_4PO_4·7H_2O$.

TGA/DSC Analysis of Mechanochemically Derived Double Salts. The TGA and DSC temperature profiles obtained of the samples prepared via mechanochemical treatment of Ca- and Mg-bearing minerals and MAP are shown in Figure 5 compared to those of MAP. Samples synthesized from the corresponding Ca- and Mg-hydroxides were utilized. The left panel of Figure 5 shows TGA and DSC profiles of the complex double salts of Mg and Ca ($Ca(NH_4)_2(HPO_4)_2·H_2O$ and $Mg(NH_4)_2(HPO_4)_2·4H_2O$), while the right panel shows those of Ca- and Mg-struvite ($CaNH_4PO_4·H_2O$ and $MgNH_4PO_4·6H_2O$). MAP exhibited two endothermic peaks at 210 and 620 °C with the

DOI: 10.1021/acssuschemeng.8b06129
ACS Sustainable Chem. Eng. 2019, 7, 6802−6812

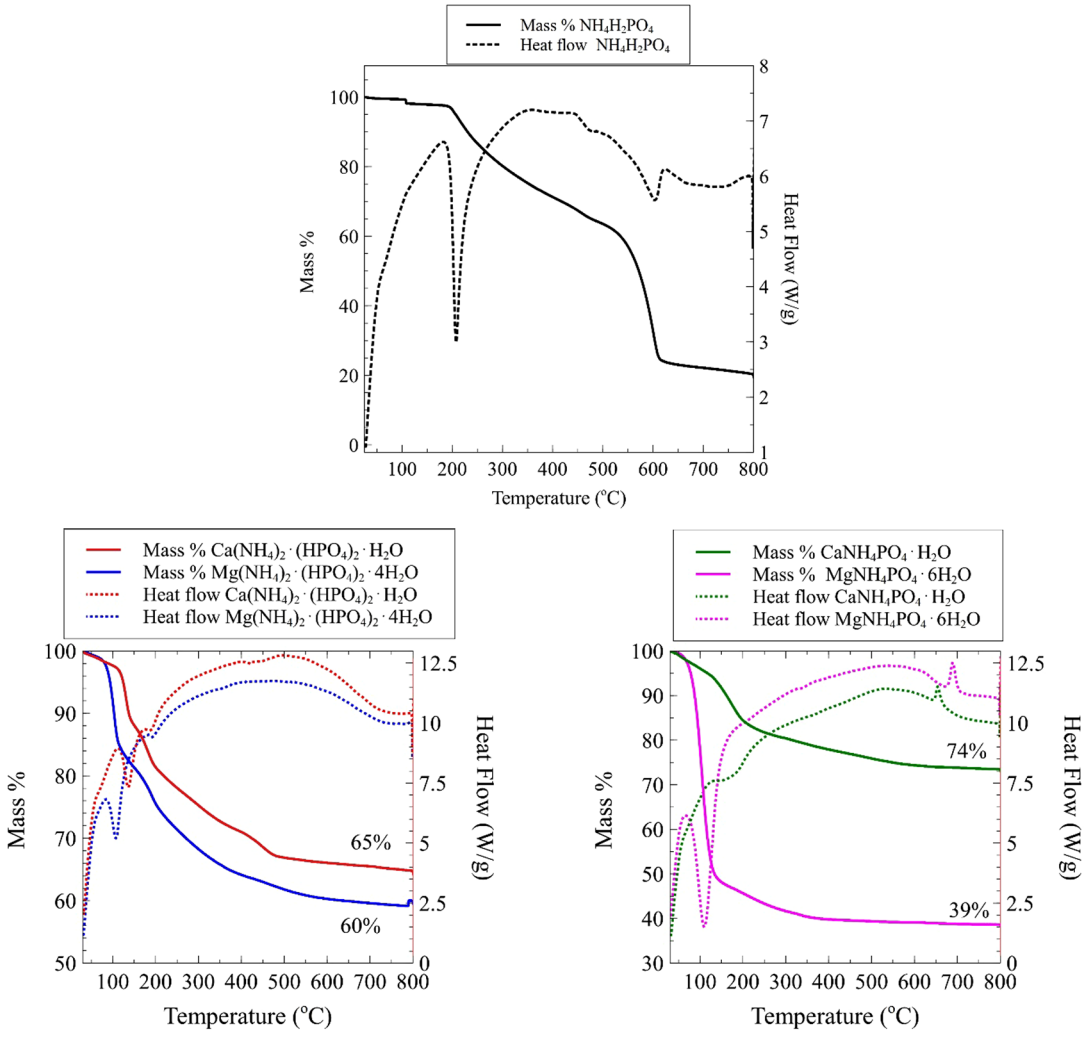

Figure 5. TGA and DSC temperature profiles obtained of the samples prepared via mechanochemical treatment of Ca- and Mg-bearing minerals and MAP. The left panel shows TGA and DSC profiles of the complex double salts of Mg and Ca ($Ca(NH_4)_2(HPO_4)_2 \cdot H_2O$ and $Mg(NH_4)_2(HPO_4)_2 \cdot 4H_2O$), while the right panel shows those of Ca- and Mg-struvite ($CaNH_4PO_4 \cdot H_2O$ and $MgNH_4PO_4 \cdot 6H_2O$). TGA and DSC temperature profiles of MAP are shown for reference.

corresponding sharp mass losses. The first mass loss is assigned to the MAP decomposition with ionic fragments of NH_3 detected in the gas phase using mass spectrometry.[65] The high temperature peak is due to the very complex decomposition mechanism of H_3PO_4 into pyrophosphoric acid and water followed by pyrophosphoric acid into methaphosphoric acid and water, respectively.[65,66] Only Mg-struvite ($MgNH_4PO_4 \cdot 6H_2O$) has been extensively characterized in the literature[67,68] so thermal data interpretation of other salts was done by comparison.

In particular, the TGA temperature profiles of the complex double salts ($Ca(NH_4)_2 \cdot (HPO_4)_2 \cdot H_2O$ and $Mg(NH_4)_2 \cdot (HPO_4)_2 \cdot 4H_2O$) showed that the samples began to dehydrate and lose their mass already above room temperature. This dehydration continued until 150 °C, after which the decomposition of the crystalline samples began with the release of NH_3. The dehydration event is also marked by a sharp peak in DSC profiles at 138 °C in $Ca(NH_4)_2(HPO_4) \cdot H_2O$ and at 105 °C in $Mg(NH_4)_2 \cdot (HPO_4) \cdot 6H_2O$, respectively. Moreover, the decomposition of samples with release of NH_3 are marked by smaller peaks in the DSC profiles at 190 °C for both compounds. The decomposition continued until ~500–600 °C for both the double salts, after which no further major loss in mass was observed. The final mass of $Ca(NH_4)_2 \cdot (HPO_4)_2 \cdot H_2O$ and $Mg(NH_4)_2 \cdot (HPO_4)_2 \cdot 4H_2O$ was 65% and 60% of the initial masses, respectively. No other peaks, thus no other phase transitions, were observed in the DSC profiles of both complex double salts. Among the two double salts, $Ca(NH_4)_2 \cdot (HPO_4) \cdot H_2O$ proved to be more thermally stable in this thermal analysis.

On the other hand, the TGA of the Ca- and Mg-containing struvite showed that dehydration onset slightly above the room temperature. This dehydration continued up to ~100 °C, after which the decomposition of the crystalline samples began with the release of NH_3. The decomposition continued until ~500–600 °C for $CaNH_4PO_4 \cdot H_2O$ and ~350 °C for $MgNH_4PO_4 \cdot 6H_2O$, after which no further major loss in mass was observed. The final mass of $CaNH_4PO_4 \cdot H_2O$ and $MgNH_4PO_4 \cdot 6H_2O$ was 74% and 39% of the initial mass, respectively. The exact decomposition product was not identified due to a very complex pathway involving many phosphorus species, such as ortho-, pyro-, and triphosphates.[69] The dehydration event corresponded to a sharp peak in the DSC profile of $MgNH_4PO_4 \cdot 6H_2O$ at 108 °C. However, no such pronounced

DOI: 10.1021/acssuschemeng.8b06129
ACS Sustainable Chem. Eng. 2019, 7, 6802–6812

peak was observed in the $CaNH_4PO_4·H_2O$, which only exhibited a broad DSC shoulder at 186 °C. However, unlike the double salts, Ca- and Mg-containing struvite also exhibited two exothermic DSC bands at 651 and 689 °C, respectively. These exothermic DSC peaks were also reported for $MgNH_4PO_4·H_2O$ in the literature.[70,71] Among the two struvites, $CaNH_4PO_4·H_2O$ proved to be much more thermally stable.

Raman Spectroscopy Analysis of Mechanochemically Derived Double Salts. All the double salts obtained exhibit Raman bands due to the NH_4^+, PO_4^{3-}, and HPO_4^{2-} ions as shown in Figure 6. Raman spectroscopy is especially suited for ammonium and phosphate containing salt analysis since it is very sensitive to symmetric vibrations of the relevant ions, including PO_4^{3-}.[72] Accordingly, symmetric stretch, $\nu_1(PO_4^{3-})$, of MAP was observed at 925 cm^{-1} consistent with the literature.[73] The main peak for PO_4^{3-} observed in all double salts shifted to higher wavenumbers signifying a change in binding configuration from that of MAP. Ca- and Mg-struvite shifts are 16 and 22 cm^{-1} while they are −46 and 53 cm^{-1} for Ca- and Mg-complex double salts, respectively. In addition $\nu_2(NH_4^+)$ of MAP was detected at 1664 cm^{-1}. Both of the bands are shifted from those of free PO_4^{3-} and NH_4^+ at 936 and 1685 cm^{-1}, respectively, indicating a distortion in the tetrahedron groups related to the deviation from the T_d symmetry.[73] In the previous work it was shown that Mg–struvite samples synthesized using aqueous NH_4^+ and PO_4^{3-} precursors and water-soluble $MgCl_2$ exhibited a Raman PO_4^{3-} band at 950 cm^{-1} due to the symmetric PO_4^{3-} stretch.[72] Two prominent peaks in 1400−1700 cm^{-1} region were assigned to the deformational vibrations of NH_4^+ tetrahedra.[74] This is consistent with the spectral features shown in Figure 6 for $MgNH_4PO_4·6H_2O$.

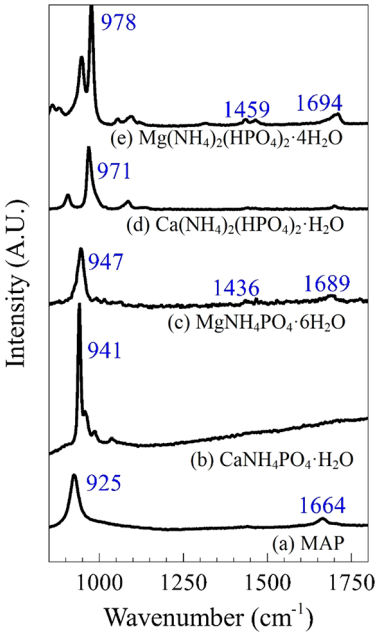

Figure 6. Raman spectra of (a) MAP, (b) $CaNH_4PO_4·H_2O$, (c) $MgNH_4PO_4·6H_2O$, (d) $Ca(NH_4)_2·(HPO_4)_2·H_2O$, and (e) $Mg(NH_4)_2·(HPO_4)_2·4H_2O$ mechanochemically synthesized using $Ca(OH)_2$ and $Mg(OH)_2$.

Spectral characterization, let alone the exact crystalline structure, of other compounds, namely, $CaNH_4PO_4·H_2O$, $Ca(NH_4)_2(HPO_4)_2·H_2O$, and $Mg(NH_4)_2(HPO_4)_2·4H_2O$ is not present in the literature. Takagi et al.[75] reported the crystal structure of $CaNH_4PO_4·7H_2O$ and noted this highly hydrated crystal as very unstable as it began decomposing at room temperature. We did not notice any change to the pXRD pattern of $CaNH_4PO_4·H_2O$ with time with the stable Raman peak at 941 cm^{-1}. Bands to the higher wavenumber side can be assigned to the asymmetric PO_4^{3-} bands activated in Raman due to the distorted geometry. Bands due to NH_4^+ were not observed in the 1400−1700 cm^{-1} region. This is potentially due to the degradation and disorder that is introduced during the milling.[76−78] In general, loss of the peak vibrational degeneracy and any structural vibrations in mechanochemically processed minerals, such as kaolinite, has previously been observed.[78]

A much more complex vibrational structure is expected in the phosphate stretching region of complex double salts,

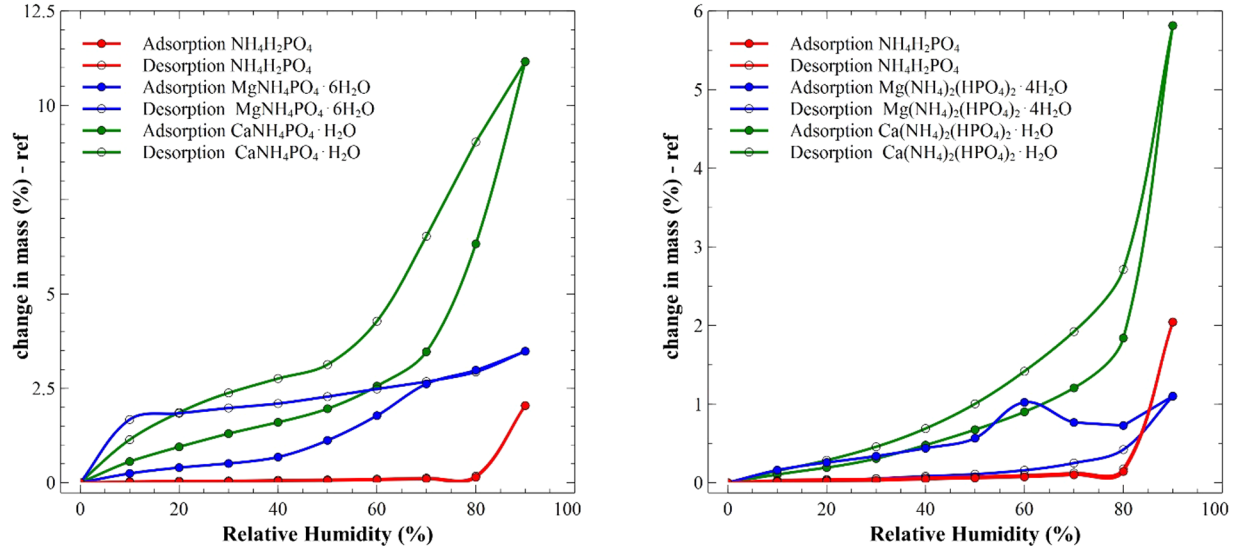

Figure 7. Adsorption/desorption curves (left) $MgNH_4PO_4·6H_2O$ and $CaNH_4PO_4·H_2O$ and (right) $Mg(NH_4)_2·(HPO_4)_2·4H_2O$ and $Ca(NH_4)_2·(HPO_4)_2·H_2O$ compared to MAP. Adsorbed water amount is normalized to the reference which is the dry sample.

DOI: 10.1021/acssuschemeng.8b06129
ACS Sustainable Chem. Eng. 2019, 7, 6802−6812

$Ca(NH_4)_2(HPO_4)_2{\cdot}H_2O$ and $Mg(NH_4)_2(HPO_4)_2{\cdot}4H_2O$, since Ca- and Mg-struvites possess PO_4^{3-} functional groups while complex double salts possess HPO_4^{2-}, potentially in two binding environments. Ability to differentiate between HPO_4^{2-} and PO_4^{3-} is also very important since it suggests that mechanochemical synthesis can lead to either protonated or unprotonated anions depending on the stoichiometry and the thermodynamic stability of the products. Importantly, protonation of PO_4^{3-} should lead to additional bands due to decrease of vibrational symmetry and activate PO antisymmetric stretching vibrations of HPO_4^{2-}.[79] A major peak at 978 cm^{-1} for $Mg(NH_4)_2(HPO_4)_2{\cdot}4H_2O$ is in agreement with that of newberyite mineral, $Mg(HPO_4){\cdot}3H_2O$, at 982 cm^{-1} assigned to the ν_1 (PO_4^{3-}) symmetric stretching mode.[80] Additional peaks are present and can be attributed to two different binding environments in the crystals. It is particularly pronounced in the case of $Mg(NH_4)_2(HPO_4)_2{\cdot}4H_2O$ with peaks at 1459 and 1694 cm^{-1} split into doublets. Multiple peaks in $Ca(NH_4)_2(HPO_4)_2{\cdot}H_2O$ spectrum centered around 971 cm^{-1} suggest the presence of HPO_4^{2-} ions.

Dynamic Vapor Sorption Measurements of Double Salts. The amount of the adsorbed water and solid double salt response to changes in relative humidity were investigated using constant temperature adsorption/desorption experiments by varying water as relative humidity. Results are shown in Figure 7. The relative humidity (RH) here is defined as where P_o is the saturated vapor pressure of water at 298 K and 1 atm and P is the actual water pressure at the same temperature and pressure according to

$$\mathrm{RH}(\%) = \frac{P}{P_o}100 \tag{13}$$

In particular, MAP adsorbs a little less water than $MgNH_4PO_4{\cdot}6H_2O$ at the highest RH and ~11 times less than $CaNH_4PO_4{\cdot}H_2O$. Interestingly, in both cases, calcium double salt adsorbed more RH than the corresponding magnesium double salt. Increase in RH adsorbed content can be qualitatively correlated with the reported high solubility.[48] MAP DVS data exhibited no hysteresis between the adsorption and desorption branches. A sharp increase in adsorbed water content of MAP at 80% RH is assigned to its deliquescence point. This suggests that MAP particles adsorb and desorb water as RH without becoming supersaturated solutions. All of the double salts shown in Figure 7 exhibited large hysteresis between the adsorption and desorption curves. In particular, during the increase in RH after the deliquescence point, the aqueous layers were formed via a continuous hygroscopic growth. During the dehydration step, the representative hydrated particles lacked a distinct efflorescence point as exhibited by a continuous hysteresis down to low (<10% RH) values of a desorption branch. The direct absence of an observable efflorescence point after deliquescence is reached, suggests that some water remains bound in a structural form (H-bonded or in a monolayer form), especially at low RH. Further, water, still bound at intermediate RH (70 to 30%), can be regarded as the continuous transition of the bound-to-free water with the vaporization enthalpy slightly higher than that for pure water.[81] It potentially indicates that strong hydrogen bonds were formed between a double salt surface and adsorbed water molecules. Considering that double salts are water-soluble, crystalline phase transitions under high RH can be inferred. This can be seen in a particular example of $Mg(NH_4)_2(HPO_4)_2{\cdot}4H_2O$ as shown in Figure 7 right. The adsorption branch undergoes an unexpected temporary mass increase at 60%. Surprisingly, the desorption branch then has lower adsorbed RH content which is a very unusual phenomenon. This suggests that if exposed to 90% RH, $Mg(NH_4)_2(HPO_4)_2{\cdot}4H_2O$ transforms into another, unidentified phase. In general, desorption curves in all materials appear to be significantly diffusion limited. Effectively, the moisture gets "trapped" into the bulk of the sample and becomes very hard to desorb. After the sample deliquesces, it essentially dissolves into solution with the water. This is particularly true in DVS measurements where a small amount of material (~5 mg) is utilized. Overall, the DVS data suggest that the resulting double salt materials are more moisture sensitive than the main reactant MAP.

CONCLUSIONS AND SUSTAINABILITY IMPLICATIONS

This work focuses on a synthesis via grinding process to form double salts such as $Ca(NH_4)_2(HPO_4)_2{\cdot}H_2O$ dimorph B and $Mg(NH_4)_2(HPO_4)_2{\cdot}4H_2O$ dimorph A, the individual polymorphs with high water solubility, using MAP as N and P source. In addition, Ca- and Mg-struvites, that is, $CaNH_4PO_4{\cdot}H_2O$ and $MgNH_4PO_4{\cdot}6H_2O$, have also been synthesized using the same precursors by adjusting the reactant ratio. In this study, these compounds were created from insoluble common calcium and magnesium minerals, such as hydroxides, carbonates, and oxides. Interestingly though, the reactions also needed water content via LAG to form the product even though product stoichiometry did not require it, and solubility of the precursor played an important role in the product formation. Furthermore, unexpected behavior was observed; $Ca(OH)_2$ transformed into $Ca(NH_4)_2(HPO_4)_2{\cdot}H_2O$ with or without LAG, suggesting that it can behave as a hydrated reactive intermediate during CaO and $CaCO_3$ conversion. Further *in situ* mechanochemical experiments are underway to elucidate the exact nature of the reactive intermediate during the conversion of Ca- and Mg-hydroxides, oxides, and carbonates into water-soluble salts.

Ca- and Mg-are commonly found in many types of sedimentary and igneous rock; additionally, carbonate sedimentary rock on Earth has around 349 300 ppm of calcium and magnesium combined (excluding the carbonate CO_3 anion).[82] It is an improved synthesis method since the original synthesis using precipitation from aqueous solution of calcium carbonate and ammonium phosphate needed days-to-weeks to yield $Ca(NH_4)_2(HPO_4)_2{\cdot}H_2O$ dimorph B,[47] while mechanochemical synthesis is orders of magnitude faster. Additionally, both $Ca(NH_4)_2(HPO_4)_2{\cdot}H_2O$ dimorphs have nutrient content similar to that of commercially available and highly utilized ammoniated triple superphosphate that contains 4 pounds of N per unit of P_2O_5, but, unlike the ammoniated superphosphate, these complex double salts release both their N and P into the soil slowly and from a single source.[47] Decreased N and P release would lead to higher nutrient availability for the plants, which is imperative, given the exponential growth in anthropogenic activity.

Moreover, groundwater contamination and eutrophication of freshwater and coastal ecosystems[8] would potentially be reduced as well as tropospheric pollution with N containing gases such as NH_3 and the main NO_x compounds. N_2O is a potent greenhouse gas with 300 times the heat-trapping capacity of CO_2[83] that depletes stratospheric ozone.[84−87] High $NO+NO_2$ emissions from fertilized soils have been shown to

DOI: 10.1021/acssuschemeng.8b06129
ACS Sustainable Chem. Eng. 2019, 7, 6802−6812

increase the concentration of harmful tropospheric ozone. In terms of energy demand, because the process to synthesize ammonia (NH_3), a reactant used to make major N-fertilizer, urea, remains energy intensive and uses up to 1% of the global energy and ∼4% of natural gas,[14,88,89] slower nutrient release will decrease the need of the mineral fertilizer influx and hence the energy consumed in their production.

AUTHOR INFORMATION

Corresponding Author

*E-mail: job314@lehigh.edu. Tel.: +1-610-758-6836.

ORCID

Jonas Baltrusaitis: 0000-0001-5634-955X

Author Contributions

L.S. performed DVS analysis, D.K. performed TGA and Raman analysis. K.H. performed mechanochemical synthesis and pXRD, J.B. conceptualized the experiments and wrote the manuscript.

Notes

The authors declare no competing financial interest.

ACKNOWLEDGMENTS

This material is based upon work supported by the National Science Foundation under Grant No. CHE 1710120. Prof. Mark Snyder is acknowledged for his help with thermogravimetric measurements.

REFERENCES

(1) Stewart, W. M.; Roberts, T. L. Food Security and the Role of Fertilizer in Supporting it. *Procedia Eng.* **2012**, *46*, 76−82.

(2) Cakmak, I. Plant nutrition research: Priorities to meet human needs for food in sustainable ways. *Plant Soil* **2002**, *247* (1), 3−24.

(3) Van Straaten, P. Farming with rocks and minerals: challenges and opportunities. *An. Acad. Bras. Cienc.* **2006**, *78* (4), 731−747.

(4) Glibert, P. M.; Maranger, R.; Sobota, D. J.; Bouwman, L. The Haber Bosch−harmful algal bloom (HB−HAB) link. *Environ. Res. Lett.* **2014**, *9* (10), 105001.

(5) Chadwick, D.; Wei, J.; Yan'an, T.; Guanghui, Y.; Qirong, S.; Qing, C. Improving manure nutrient management towards sustainable agricultural intensification in China. *Agric., Ecosyst. Environ.* **2015**, *209*, 34−46.

(6) Dimkpa, C. O.; Bindraban, P. S. Fortification of micronutrients for efficient agronomic production: a review. *Agron. Sustainable Dev.* **2016**, *36* (1), 7.

(7) Glibert, P. M.; Harrison, J.; Heil, C.; Seitzinger, S. Escalating worldwide use of urea - A global change contributing to coastal eutrophication. *Biogeochemistry* **2006**, *77* (3), 441−463.

(8) Canfield, D. E.; Glazer, A. N.; Falkowski, P. G. The Evolution and Future of Earth's Nitrogen Cycle. *Science (Washington, DC, U. S.)* **2010**, *330* (6001), 192−196.

(9) Conley, D. J.; Paerl, H. W.; Howarth, R. W.; Boesch, D. F.; Seitzinger, S. P.; Havens, K. E.; Lancelot, C.; Likens, G. E. Controlling Eutrophication: Nitrogen and Phosphorus. *Science (Washington, DC, U. S.)* **2009**, *323* (5917), 1014−1015.

(10) Galloway, J. N.; Cowling, E. B. Reactive Nitrogen and The World: 200 Years of Change. *Ambio* **2002**, *31* (2), 64−71.

(11) Duce, R. A.; LaRoche, J.; Altieri, K.; Arrigo, K. R.; Baker, A. R.; Capone, D. G.; Cornell, S.; Dentener, F.; Galloway, J.; Ganeshram, R. S.; et al. Impacts of Atmospheric Anthropogenic Nitrogen on the Open Ocean. *Science (Washington, DC, U. S.)* **2008**, *320* (5878), 893−897.

(12) Tilman, D.; Fargione, J.; Wolff, B.; D'Antonio, C.; Dobson, A.; Howarth, R.; Schindler, D.; Schlesinger, W. H.; Simberloff, D.; Swackhamer, D. Forecasting Agriculturally Driven Global Environmental Change. *Science* **2001**, *292* (5515), 281−284.

(13) Zhang, W. -f.; Dou, Z. -x.; He, P.; Ju, X.-T.; Powlson, D.; Chadwick, D.; Norse, D.; Lu, Y.-L.; Zhang, Y.; Wu, L.; et al. New technologies reduce greenhouse gas emissions from nitrogenous fertilizer in China. *Proc. Natl. Acad. Sci. U. S. A.* **2013**, *110* (21), 8375−8380.

(14) Baltrusaitis, J. Sustainable Ammonia Production. *ACS Sustainable Chem. Eng.* **2017**, *5* (11), 9527−9527.

(15) Baltrusaitis, J.; Sviklas, A. M. From Insoluble Minerals to Liquid Fertilizers: Magnesite as a Source of Magnesium (Mg) Nutrient. *ACS Sustainable Chem. Eng.* **2016**, *4* (10), 5404−5408.

(16) Sharma, L.; Brigaityte, O.; Honer, K.; Kalfaoglu, E.; Slinksiene, R.; Streimikis, V.; Sviklas, A. M.; Baltrusaitis, J. Carnallite-derived solid waste as potassium (K) and magnesium (Mg) source in granulated compound NPK fertilizers. *ACS Sustainable Chem. Eng.* **2018**, *6*, 9427.

(17) Honer, K.; Pico, C.; Baltrusaitis, J. Reactive Mechanosynthesis of Urea Ionic Cocrystal Fertilizer Materials from Abundant Low Solubility Magnesium- and Calcium-Containing Minerals. *ACS Sustainable Chem. Eng.* **2018**, *6* (4), 4680−4687.

(18) Sanchez, P. A. Soil Fertility and Hunger in Africa. *Science (Washington, DC, U. S.)* **2002**, *295*, 2019−2020.

(19) Casali, L.; Mazzei, L.; Shemchuk, O.; Honer, K.; Grepioni, F.; Ciurli, S.; Braga, D.; Baltrusaitis, J. Smart Urea Ionic Co-crystals with Enhanced Urease Inhibition Activity for Improved Nitrogen Cycle Management. *Chem. Commun.* **2018**, *54*, 7637.

(20) Leonardos, O. H.; Fyfe, W. S.; Kronberg, B. I. The Use of Ground Rocks in Laterite Systems: An Improvement to the Use of Conventional Soluble Fertilizers? *Chem. Geol.* **1987**, *60*, 361−370.

(21) True, R. H. The Significance of Calcium for Higher Green Plants. *Science (Washington, DC, U. S.)* **1922**, *55* (1410), 1−6.

(22) Wyatt, F. A. The Influence of Calcium and Magnesium Compounds on Plant Growth. *J. Agric. Res.* **1916**, *6* (16), 589−618.

(23) Hepler, P. K.; Winship, L. J. Calcium at the cell wall-cytoplast interface. *J. Integr. Plant Biol.* **2010**, *52* (2), 147−160.

(24) Shaul, O. Magnesium transport and function in plants: the tip of the iceberg. *BioMetals* **2002**, *15* (3), 309−323.

(25) Senbayram, M.; Gransee, A.; Wahle, V.; Thiel, H. Role of magnesium fertilisers in agriculture: plant−soil continuum. *Crop Pasture Sci.* **2015**, *66* (12), 1219.

(26) Römheld, V.; Kirkby, E. A. Research on potassium in agriculture: needs and prospects. *Plant Soil* **2010**, *335* (1), 155−180.

(27) Timilsena, Y. P.; Adhikari, R.; Casey, P.; Muster, T.; Gill, H.; Adhikari, B. Enhanced efficiency fertilisers: a review of formulation and nutrient release patterns. *J. Sci. Food Agric.* **2015**, *95* (6), 1131−1142.

(28) James, S. L.; Adams, C. J.; Bolm, C.; Braga, D.; Collier, P.; Friscic, T.; Grepioni, F.; Harris, K. D. M.; Hyett, G.; Jones, W.; et al. Mechanochemistry: opportunities for new and cleaner synthesis. *Chem. Soc. Rev.* **2012**, *41* (1), 413−447.

(29) Boldyrev, V. V. Mechanochemistry and mechanical activation of solids. *Russ. Chem. Rev.* **2006**, *75* (3), 177−189.

(30) Gutman, E. M. *Mechanochemistry of Materials*; Cambridge International Science Publishing: 1998.

(31) Boldyrev, V. V. Mechanochemistry and mechanical activation of solids. *Solid State Ionics* **1993**, *63−65* (1−4), 537−543.

(32) Wood, S.; Cowie, A. *A Review of Greenhouse Gas Emission Factors for Fertiliser Production*: Research and Development Division, State Forests of New South Wales. Cooperative Research Centre for Greenhouse Accounting: 2004.

(33) Kramer, K. J.; Moll, H. C.; Nonhebel, S. Total greenhouse gas emissions related to the Dutch crop production system. *Agric., Ecosyst. Environ.* **1999**, *72*, 9−16.

(34) Fuerstenau, D. W.; Abouzeid, A. M. The energy efficiency of ball milling in comminution. *Int. J. Miner. Process.* **2002**, *67*, 161−185.

(35) Ballantyne, G. R.; Peukert, W.; Powell, M. S. Size specific energy (SSE) — required to generate minus 75 micron material. *Int. J. Miner. Process.* **2015**, *136*, 2−6.

(36) Zhang, Q.; Saito, F.; Solihin. Mechanochemical Synthesis of Slow-Release Fertilizers through Incorporation of Alumina Compo-

DOI: 10.1021/acssuschemeng.8b06129
ACS Sustainable Chem. Eng. 2019, 7, 6802−6812

sition into Potassium/Ammonium Phosphates. *J. Am. Ceram. Soc.* **2009**, *92* (12), 3070−3073.
(37) Borges, R.; Prevot, V.; Forano, C.; Wypych, F. Design and Kinetic Study of Sustainable Potential Slow-Release Fertilizer Obtained by Mechanochemical Activation of Clay Minerals and Potassium Monohydrogen Phosphate. *Ind. Eng. Chem. Res.* **2017**, *56* (3), 708−716.
(38) Solihin; Zhang, Q.; Tongamp, W.; Saito, F. Mechanochemical synthesis of kaolin−KH2PO4 and kaolin−NH4H2PO4 complexes for application as slow release fertilizer. *Powder Technol.* **2011**, *212* (2), 354−358.
(39) Intasa-Ard, S. G.; Imwiset, K. J.; Bureekaew, S.; Ogawa, M. Mechanochemical methods for the preparation of intercalation compounds, from intercalation to the formation of layered double hydroxides. *Dalt. Trans.* **2018**, *47* (9), 2896−2916.
(40) Tongamp, W.; Zhang, Q.; Saito, F. Mechanochemical route for synthesizing nitrate form of layered double hydroxide. *Powder Technol.* **2008**, *185* (1), 43−48.
(41) Yuan, W.; Solihin; Zhang, Q.; Kano, J.; Saito, F. Mechanochemical formation of K−Si−Ca−O compound as a slow-release fertilizer. *Powder Technol.* **2014**, *260*, 22−26.
(42) Said, A.; Zhang, Q.; Qu, J.; Liu, Y.; Lei, Z.; Hu, H.; Xu, Z. Mechanochemical activation of phlogopite to directly produce slow-release potassium fertilizer. *Appl. Clay Sci.* **2018**, *165*, 77−81.
(43) Borges, R.; Baika, L. M.; Grassi, M. T.; Wypych, F. Mechanochemical conversion of chrysotile/K 2 HPO 4 mixtures into potential sustainable and environmentally friendly slow-release fertilizers. *J. Environ. Manage.* **2018**, *206*, 962−970.
(44) Li, X.; Lei, Z.; Qu, J.; Li, Z.; Zhou, X.; Zhang, Q. Synthesizing slow-release fertilizers via mechanochemical processing for potentially recycling the waste ferrous sulfate from titanium dioxide production. *J. Environ. Manage.* **2017**, *186*, 120−126.
(45) Solihin; Zhang, Q.; Tongamp, W.; Saito, F. Mechanochemical Route for Synthesizing KMgPO4 and NH4MgPO4 for Application as Slow-Release Fertilizers. *Ind. Eng. Chem. Res.* **2010**, *49* (5), 2213−2216.
(46) Honer, K.; Kalfaoglu, E.; Pico, C.; McCann, J.; Baltrusaitis, J. Mechanosynthesis of Magnesium and Calcium Salt−Urea Ionic Cocrystal Fertilizer Materials for Improved Nitrogen Management. *ACS Sustainable Chem. Eng.* **2017**, *5* (10), 8546−8550.
(47) Frazier, A. W.; Lehr, J. R.; Smith, J. P. Fertilizer Reaction, Calcium Ammonium Orthophosphates. *J. Agric. Food Chem.* **1964**, *12* (3), 198−201.
(48) Frazier, A. W.; Lehr, J. R.; Smith, J. P. Calcium Ammonium Orthophosphates. *J. Agric. Food Chem.* **1964**, *12* (3), 198−201.
(49) Dillard, E. F.; Frazier, A. W.; Woodis, T. C.; Achorn, F. P. Precipitated Impurities in 18−46-O Fertilizers Prepared from Wet-Process Phosphoric Acid. *J. Agric. Food Chem.* **1982**, *30* (2), 382−388.
(50) Frazier, A. W.; Waerstad, K. J. The Phase System MgO-(NH4)2O-P2O5-H2O at 25C. *Ind. Eng. Chem. Res.* **1992**, *31* (8), 2066−2068.
(51) Frazier, A. W. Fluid Fertilizers. In *Fluid Fertilizers*; Potts, J. M., Ed.; Muscle Shoals: AL, 1984; p 32.
(52) Bell, L. C.; Black, C. A. Crystalline Phosphates Produced By Interaction of Orthophosphate Fertilizers With Slightly Acid and Alkaline Soils. *Soil Sci. Soc. Am. J.* **1970**, *34*, 735−740.
(53) Martini, J. E. J. Swaknoite [Ca(NH4)2(HPO4)2 H2O, orthorhombic]: a new mineral from Arnhem cave, Namibia. *Bull. South African Speleol. Assoc.* **1991**, *32*, 72−74.
(54) Frazier, A. W.; Smith, J. P.; Lehr, J. R. Precipitated Impurities in Fertilizers Prepared from Wet-Process Phosphoric Acid. *J. Agric. Food Chem.* **1966**, *14*, 522−529.
(55) Frazier, A. W.; Scheib, R. M.; Thrasher, R. D. Clarification of Ammonium Polyphosphate Fertilizer Solutions Wet-process. *J. Agric. Food Chem.* **1972**, *20* (1), 138−145.
(56) Frazier, A. W.; Dillard, E. F. Solubilities in the System Magnesium Oxide-Ammonia-Orthophosphoric Acid-Pyrophosphoric Acid-Water at 25° C. *J. Agric. Food Chem.* **1981**, *29* (1), 160−162.
(57) Frazier, A. W.; Dillard, E. F.; Thrasher, R. D.; Waerstad, K. R. The System NH3K2O-H3PO4-H4P2O7H2O at 25°. *J. Agric. Food Chem.* **1973**, *21* (4), 700−704.
(58) Frazier, A. W.; Smith, J. P.; Lehr, J. R. The magnesium phosphates hannayite, schertelite and bobierrite. *Am. Mineral.* **1963**, *48* (5−6), 635−641.
(59) Frazier, A. W.; Waerstad, K. J. The phase system magnesia-ammonium oxide-phosphorus oxide-water at 25.degree. C. *Ind. Eng. Chem. Res.* **1992**, *31* (8), 2065−2068.
(60) Abbona, F.; Calleri, M.; Ivaldi, G. Synthetic struvite, MgNH4PO4 × 6H2O: correct polarity and surface features of some complementary forms. *Acta Crystallogr., Sect. B: Struct. Sci.* **1984**, *40* (3), 223−227.
(61) Losev, E. A.; Boldyreva, E. V. The role of a liquid in "dry" co-grinding: a case study of the effect of water on mechanochemical synthesis in a "l-serine-oxalic acid" system. *CrystEngComm* **2014**, *16* (19), 3857−3866.
(62) Friscic, T.; Fabian, L. Mechanochemical conversion of a metal oxide into coordination polymers and porous frameworks using liquid-assisted grinding (LAG). *CrystEngComm* **2009**, *11* (5), 743−745.
(63) Karki, S.; Friščić, T.; Jones, W.; Motherwell, W. D. S. Screening for pharmaceutical cocrystal hydrates via neat and liquid-assisted grinding. *Mol. Pharmaceutics* **2007**, *4* (3), 347−354.
(64) Howard, J. L.; Sagatov, Y.; Repusseau, L.; Schotten, C.; Browne, D. L. Controlling reactivity through liquid assisted grinding: the curious case of mechanochemical fluorination. *Green Chem.* **2017**, *19* (12), 2798−2802.
(65) Pardo, A.; Romero, J.; Ortiz, E. High-temperature behaviour of ammonium dihydrogen phosphate. *J. Phys.: Conf. Ser.* **2017**, *935* (1), 12050.
(66) Modolo, L. V.; Da-Silva, C. J.; Brandão, D. S.; Chaves, I. S. A minireview on what we have learned about urease inhibitors of agricultural interest since mid-2000s. *J. Adv. Res.* **2018**, *13*, 29.
(67) Sarkar, A. K. Hydration/dehydration characteristics of struvite and dittmarite pertaining to magnesium ammonium phosphate cement systems. *J. Mater. Sci.* **1991**, *26* (9), 2514−2518.
(68) Frost, R. L.; Weier, M. L.; Erickson, K. L. Thermal decomposition of struvite. *J. Therm. Anal. Calorim.* **2004**, *76* (3), 1025−1033.
(69) Lapina, L. M. Metal Ammonium Phosphates and Their New Applications. *Russ. Chem. Rev.* **1968**, *37* (9), 693.
(70) Rathod, K. R.; Jogiya, B. V.; Chauhan, C. K.; Joshi, M. J. Synthesis and characterization of struvite nano particles. *AIP Conf. Proc.* **2014**, *050131*, 050131.
(71) Chauhan, C. K.; Joshi, M. J. In vitro crystallization, characterization and growth-inhibition study of urinary type struvite crystals. *J. Cryst. Growth* **2013**, *362* (1), 330−337.
(72) Kirinovic, E.; Leichtfuss, A. R.; Navizaga, C.; Zhang, H.; Christus, J. D. S.; Baltrusaitis, J. Spectroscopic and microscopic identification of the reaction products and intermediates during the struvite (MgNH4PO4·6H2O) formation from magnesium oxide (MgO) and magnesium carbonate (MgCO3) microparticles. *ACS Sustainable Chem. Eng.* **2017**, *5* (2), 1567−1577.
(73) Ben Brahim, F.; Bulou, A. Growth and spectroscopy studies of ADP single crystals with l-glutamine and l-cysteine amino acids. *Vib. Spectrosc.* **2013**, *65*, 176−185.
(74) Prywer, J.; Kasprowicz, D.; Runka, T. Temperature-dependent μ-Raman investigation of struvite crystals. *Spectrochim. Acta, Part A* **2016**, *158*, 18−23.
(75) Takagi, S.; Mathew, M.; Brown, W. E. Structure of ammonium calcium phosphate heptahydrate, Ca(NH4)PO4.7H2O. *Acta Crystallogr., Sect. C: Cryst. Struct. Commun.* **1984**, *40* (7), 1111−1113.
(76) Šepelák, V.; Düvel, A.; Wilkening, M.; Becker, K.-D.; Heitjans, P. Mechanochemical reactions and syntheses of oxides. *Chem. Soc. Rev.* **2013**, *42* (18), 7507.
(77) Šepelák, V.; Steinike, U.; Uecker, D. C.; Wißmann, S.; Becker, K. D. Structural Disorder in Mechanosynthesized Zinc Ferrite. *J. Solid State Chem.* **1998**, *135* (1), 52−58.

DOI: 10.1021/acssuschemeng.8b06129
ACS Sustainable Chem. Eng. 2019, 7, 6802−6812

(78) Aglietti, E. F.; Porto Lopez, J. M.; Pereira, E. Mechanochemical effects in kaolinite grinding. II. Structural aspects. *Int. J. Miner. Process.* **1986**, *16* (1−2), 135−146.
(79) Frost, R. L.; Xi, Y.; Scholz, R.; López, A.; Belotti, F. M. Vibrational spectroscopic characterization of the phosphate mineral hureaulite − (Mn, Fe)5(PO4)2(HPO4)2·4(H2O). *Vib. Spectrosc.* **2013**, *66*, 69−75.
(80) Frost, R. L.; Weier, M. L.; Martens, W. N.; Henry, D. A.; Mills, S. J. Raman spectroscopy of newberyite, hannayite and struvite. *Spectrochim. Acta, Part A* **2005**, *62* (1−3), 181−188.
(81) Basu, S.; Shivhare, U. S.; Mujumdar, A. S. Models for Sorption Isotherms for Foods: A Review. *Drying Technol.* **2006**, *24* (8), 917−930.
(82) Turekian, K. K.; Wedepohl, K. H. Distribution of the Elements in Some Major Units of the Earth's Crust. *Geol. Soc. Am. Bull.* **1961**, *72* (2), 175−192.
(83) Coskun, D.; Britto, D. T.; Shi, W.; Kronzucker, H. J. Nitrogen transformations in modern agriculture and the role of biological nitrification inhibition. *Nat. Plants* **2017**, *3*, 17074.
(84) Zhang, X.; Davidson, E. A.; Mauzerall, D. L.; Searchinger, T. D.; Dumas, P.; Shen, Y. Managing nitrogen for sustainable development. *Nature* **2015**, *528*, 51.
(85) Hewitt, C. N.; MacKenzie, A. R.; Di Carlo, P.; Di Marco, C. F.; Dorsey, J. R.; Evans, M.; Fowler, D.; Gallagher, M. W.; Hopkins, J. R.; Jones, C. E.; et al. Nitrogen management is essential to prevent tropical oil palm plantations from causing ground-level ozone pollution. *Proc. Natl. Acad. Sci. U. S. A.* **2009**, *106* (44), 18447−18451.
(86) Galloway, J. N.; Aber, J. D.; Erisman, J. W.; Seitzinger, S. P.; Howarth, R. W.; Cowling, E. B.; Cosby, B. J. The Nitrogen Cascade. *BioScience* **2003**, *53* (4), 341−356.
(87) Galloway, J. N.; Dentener, F. J.; Capone, D. G.; Boyer, E. W.; Howarth, R. W.; Seitzinger, S. P.; Asner, G. P.; Cleveland, C. C.; Green, P. A.; Holland, E. A.; et al. Nitrogen Cycles: Past, Present, and Future. *Biogeochemistry* **2004**, *70* (2), 153−226.
(88) Patil, B. S.; Wang, Q.; Hessel, V.; Lang, J. Plasma N2-fixation: 1900−2014. *Catal. Today* **2015**, *256*, 49−66.
(89) Erisman, J. W.; Sutton, M. A.; Galloway, J.; Klimont, Z.; Winiwarter, W. How a century of ammonia synthesis changed the world. *Nat. Geosci.* **2008**, *1* (10), 636−639.

DOI: 10.1021/acssuschemeng.8b06129
ACS Sustainable Chem. Eng. 2019, 7, 6802−6812